Iterative image reconstruction using prior knowledge

Hsin M. Shieh

Department of Electrical Engineering,

Feng Chia University,

100 Wenhwa Rd., Seatwen, Taichung, Taiwan 40724, R.O.C.

hmshieh@fcu.edu.tw

Charles L. Byrne

Department of Mathematical Sciences,

University of Massachusetts Lowell,

One University Avenue, Lowell, MA 01854, U.S.A.

Charles_Byrne@uml.edu

Markus E. Testorf

Thayer School of Engineering,

Dartmouth College,

8000 Cummings Hall, Hanover, NH 03755, U.S.A.

Markus.E.Testorf@Dartmouth.EDU

Michael A. Fiddy

Center for Optoelectronics and Optical Communications,

The University of North Carolina at Charlotte,

9201 University City Blvd., Charlotte, NC 28223, U.S.A.

mafiddy@uncc.edu

A method is proposed to reconstruct signals from incomplete data. The method, which can be interpreted both as a discrete implementation of the so-called PDFT spectral estimation technique as well as a variant of the algebraic reconstruction technique, allows one to incorporate prior information about the reconstructed signal to improve the resolution of the signal estimated. The context of diffraction tomography and image reconstruction from samples of the far field scattering amplitude are used to explore the performance of the method. Based on numerical computations the optimum choice of parameters is determined empirically by comparing image reconstructions of the non-iterative PDFT algorithm and the proposed iterative scheme.

OCIS codes: 100.3010, 100.3020, 100.3190, 100.6640, 100.6950

1. Introduction

A large number of inverse problems can be described as computing the image of an object from samples of its Fourier transformation. This includes computerized tomography and, diffraction tomography, many variants of radar imaging applications, as well as the estimate of spectra from a finite time series.

A significant problem in reconstructing an image $f(\mathbf{r})$ from finitely many projections is the limited nature of the data, allowing for non-unique solutions. The *prior discrete Fourier transform* (PDFT) method [1, 2, 3, 4, 5, 6] incorporates prior information about the image, such as support information or profile information, through the use of a weight function $p(\mathbf{r}) \geq 0$. The image obtained with the PDFT is a data consistent member of a finite-parameter family of functions of a continuous variable $\mathbf{r}$. There are as many parameters as there are data values and the parameters are determined from the data by solving a system of linear equations. The matrix involved in this system comes from the weight function $p(\mathbf{r})$. The term "PDFT" denotes the PDFT estimator in the case of Fourier transform data, where the image is computed as a product of the prior $p(\mathbf{r})$ and a discrete Fourier transformation. However, we emphasize that the PDFT is not limited to this problem, but can be applied to any data set which can be interpreted as projections in a Hilbert space which describes the experimental geometry.

Suppose $g_m(\mathbf{r})$ for $m = 1, 2, \ldots, M$ are known functions and the data vector $\mathbf{d}$ has the entries

$$d_m = \int f(\mathbf{r}) \, \overline{g_m(\mathbf{r})} \, d\mathbf{r} \, . \tag{1}$$

For $n = 1, 2, \ldots, M$ let $\mathbf{P}$ be the square matrix with entries

$$P_{mn} = \int p(\mathbf{r}) g_n(\mathbf{r}) \overline{g_m(\mathbf{r})}\, d\mathbf{r}\ , \tag{2}$$

and the vector $\mathbf{a}$ satisfy the system $\mathbf{d} = \mathbf{Pa}$. Then the PDFT estimate of the image function $f(\mathbf{r})$ is

$$\hat{f}_{PDFT}(\mathbf{r}) = p(\mathbf{r}) \sum_{n=1}^{M} a_n g_n(\mathbf{r})\ . \tag{3}$$

The cumbersome part of using the PDFT is usually the formation of the matrix $\mathbf{P}$, particularly when M is large. Our purpose, in this paper, is to illustrate how to avoid the use of this matrix. The following fact about the PDFT is the basis for our new method.

The PDFT estimate of $f(\mathbf{r})$ is the function consistent with the data whose weighted norm is minimized, where the squared weighted norm of a function $h(\mathbf{r})$ is defined to be

$$||h||^2 = \int |h(\mathbf{r})|^2 p^{-1}(\mathbf{r}) d\mathbf{r}\ . \tag{4}$$

It follows from the theory of Hilbert space that the PDFT estimate must have the form of equation (3).

The discrete PDFT (DPDFT) uses discrete representations of $f(\mathbf{r})$ and $p(\mathbf{r})$ rep-

resented by finite N by 1 vectors $\mathbf{f}$ and $\mathbf{p} > 0$, with $N > M$. The integration in equation (1) is replaced by a summation. We have

$$d_m = \sum_{n=1}^{N} A_{mn} f_n \, . \tag{5}$$

with $m = 1, ..., M$.

Vector $\mathbf{f}$ is the discrete image estimate, which satisfies $\mathbf{d} = \mathbf{A}\mathbf{f}$, and for which the squared weighted norm reads

$$||\mathbf{f}||_p^2 = \sum_{n=1}^{N} |f_n|^2 / p_n \, . \tag{6}$$

In closed form the minimum weighted norm solution is given by

$$\hat{\mathbf{f}}_{DPDFT} = \mathbf{W}^{-1}\mathbf{A}^{\dagger}(\mathbf{A}\mathbf{W}^{-1}\mathbf{A}^{\dagger})^{-1}\mathbf{d} \, , \tag{7}$$

where $\mathbf{W}$ is the diagonal matrix having the entries $1/p_n$ on the diagonal. Using the closed form to calculate the solution is not efficient for large data sets. Instead, we calculate the DPDFT solution using the *algebraic reconstruction technique* (ART) [7,8,9,10,11,12]. For the remainder of this paper we shall be concerned with the case of Fourier transform data.

The main contribution of this paper is to demonstrate that the cumbersome aspects

of the PDFT can be avoided through the DPDFT, without degrading the image resolution. It is true that, in certain cases, the matrix P may exhibit special structure, such as being Toeplitz or block-Toeplitz, and this structure can be exploited to obtain fast inversion schemes. Nevertheless, it is the actual computation of P that we wish to avoid.

2. The DPDFT

We consider the problem of estimating $f(\mathbf{r})$ from finitely many Fourier transform values, $F(\mathbf{k}_m)$ for $m = 1, 2, ..., M$. The PDFT estimator is given by

$$\hat{f}_{PDFT}(\mathbf{r}) = p(\mathbf{r}) \sum_{m=1}^{M} a_m \exp(j\mathbf{r} \cdot \mathbf{k}_m) \,, \tag{8}$$

where $p(\mathbf{r}) \geq 0$ is the prior function. The coefficients a_m for $m = 1, 2, \ldots, M$ satisfy the matrix equation

$$\mathbf{d} = \mathbf{P}\,\mathbf{a} \,, \tag{9}$$

where $\mathbf{d} = [\, F(\mathbf{k}_1), F(\mathbf{k}_2), \ldots, F(\mathbf{k}_M)\,]^T$ and $\mathbf{a} = [\, a_1, a_2, \ldots, a_M\,]^T$ are the data and coefficient column vectors, respectively, and $\mathbf{P}$ is the M by M square matrix with entries $P(\mathbf{k}_i - \mathbf{k}_j)$. Here the function $P(\mathbf{k})$ is the Fourier transform of the prior weighting function $p(\mathbf{r})$.

In many applications calculating the matrix $\mathbf{P}$ is challenging, in particular if $p(\mathbf{r})$ is not available in closed form, and the matrix elements cannot be computed from

analytic expression. In addition, solving the system of equation (9) is costly, if not impractical, for large data sets. In contrast, the DPDFT does not require the matrix $\mathbf{P}$ and it is sufficient to provide $\mathbf{p}$ as a set of discrete numerical values.

For specificity we consider the two-dimensional problem in which $f(\mathbf{r}) = f(x, y)$ and finitely many Fourier transform values of f are

$$F(\alpha_m, \beta_m) = \iint f(x, y) \exp[-j(x\alpha_m + y\beta_m)]dxdy \tag{10}$$

for $m = 1, 2, \ldots, M$. We approximate the two-dimensional integral in equation (10) using Riemann sums with $dx \approx \Delta_x, dy \approx \Delta_y$ for Δ_x, Δ_y being small enough,

$$F(\alpha_m, \beta_m) \approx \sum_{u=-U}^{U} \sum_{v=-V}^{V} f(u\Delta_x, v\Delta_y) \exp[-j(x\Delta_x\alpha_m + y\Delta_y\beta_m)]\Delta_x\Delta_y \,. \tag{11}$$

The object function $f(x, y)$ is assumed to reside entirely within the reconstructed image area, i.e. $f(x, y) = 0$ for $|x| > U\Delta_x, |y| > V\Delta_y$. With the vectorization of the double sum in equation (11), it obtains a matrix equation $\mathbf{d} = \mathbf{Af}$. The vector $\mathbf{f}$ contains the values $f(u\Delta_x, v\Delta_y)$ and the matrix $\mathbf{A}$ has $\Delta_x\Delta_y$ times the complex exponentials in the double sum for its entries.

To incorporate prior knowledge we write

$$\mathbf{Af} = \mathbf{AW}^{-\frac{1}{2}}\mathbf{W}^{\frac{1}{2}}\mathbf{f} = \mathbf{Bg} \,. \tag{12}$$

Instead of solving it in closed form, we calculate the minimum norm solution $\hat{\mathbf{g}}$ of $\mathbf{d} = \mathbf{Bg}$ using the ART. Beginning with the initial vector $\mathbf{g}^0$, the ART iterative step we set up to solve for $\hat{\mathbf{g}}$ in equation $\mathbf{d} = \mathbf{Bg}$ is given by

$$g_n^{k+1} = g_n^k + \frac{\overline{B}_{mn}\left(d_m - \sum_{i=1}^N B_{mi} g_i^k\right)}{\sum_{i=1}^N |B_{mi}|^2} \tag{13}$$

where $m = \mathrm{mod}(k, M) + 1$. The ART algorithm in equation (13) converges to $\mathbf{g}^\infty$ for which $\|\mathbf{g} - \hat{\mathbf{g}}\|$ is minimized if there exist solutions for the system of equations $\mathbf{d} = \mathbf{Bg}$. Our estimate of $\mathbf{f}$ is then $\hat{\mathbf{f}} = \mathbf{W}^{-\frac{1}{2}}\hat{\mathbf{g}}$,

$$f_n^{k+1} = f_n^k + p_n \frac{\overline{A}_{mn}\left(d_m - \sum_{i=1}^N A_{mi} f_i^k\right)}{\sum_{i=1}^N p_i |A_{mi}|^2} \ . \tag{14}$$

The estimator of equation (14) is the so-called DPDFT.

3. Convergence of the ART

The DPDFT requires finding the minimum weighted norm solution of an underdetermined system of linear equations. There are many ways to do this. In our simulations we have chosen to use the ART. We make no claims here about the best algorithm to use, but merely wish to point out the improvements in ART that can be achieved through the use of relaxation, regularization, and attention to the ordering of the equations. It is important to note that in many applications of iterative methods in image reconstruction in which time is important, only a few iterations of an iterative

algorithm may be used. Therefore, how long it takes an algorithm to converge may be less significant than how good a job it does in the first few iterative steps.

The ART algorithm can be slow to converge when the equations are ordered in an unfavorable sequence. To improve it, there have been proposals for rearranging the order in which data are accessed. By randomizing the order in which data are accessed, or by optimizing the selection order in some sense, the convergence rate can be improved dramatically [13, 14, 15]. In addition, this slow convergence can also be improved by using the relaxation method [16, 17] which provides flexibility for choosing the new estimate at each iteration during the iterative process. Applying the relaxation in the ART is that adding an adjustable parameter to the second term (projection) on the right hand side of equation (13). For the DPDFT, this manner can be written as

$$f_n^{k+1} = f_n^k + \lambda^k p_n \frac{\overline{A}_{mn}\left(d_m - \sum_{i=1}^{N} A_{mi} f_i^k\right)}{\sum_{i=1}^{N} p_i |A_{mi}|^2} \ , \tag{15}$$

where λ^k is the relaxation parameter for the k-th projection step.

To investigate the impact of rearranging and relaxation on the convergence performance of the DPDFT algorithm, we consider a two-dimensional problem of reconstructing an object function from its Fourier transform values. This demonstration particularly concentrates on one of our primary interests in developing the DPDFT algorithm for applications related to diffraction tomography. The data map in figure

1 is interpreted as the map of Fourier data which would be obtained from a bistatic radar experiment. The sampling points are equivalent to a radar frequency of $10GHz$, incident angles varying between 0^o and 355^o, and scattered field angles ranging from 0^o to 175^o, both sampled with an increment of 5^o. We emphasize, however, that only computed Fourier transform data were used to evaluate the convergence performance of the DPDFT under different environments, without the necessity to take imperfections of an experimental data acquisition step into account.

For the reconstruction we used a a circular prior function of a radius 5 cm (Figure 2(c)). The PDFT estimate in Figure 2(d) shows better resolution than the DFT estimate in Figure 2(b). The DPDFT estimate improves gradually at each iteration in accordance with the convergence characteristic of the ART [17, 18]. The DPDFT estimate after 6 iterations is shown in Figure 2(e) which is better resolved than the DFT estimate in Figure 2(b), however qualitatively the PDFT is superior. After 15 iterations the DPDFT estimate in Figure 2(f) has improved significantly and shows similar quality as compared to the PDFT estimate.

For a quantitative evaluation, we take the root mean square error (RMSE) between the object function and its estimate as a measure of the accuracy of the image reconstruction

$$RMSE = \sqrt{\frac{1}{N}\sum_{n=1}^{N} |o_n - r_n|^2} \ , \tag{16}$$

where N is the total number of pixels, and, o_n and r_n each represents the pixel

value of the object and the image, respectively. For the example in Figure 2, the RMSEs between the object and the PDFT estimate and between the object and the DPDFT estimates are shown in Figure 3(a). The characteristic of the DPDFT estimate (solid line) converges monotonically to the better solution as the number of iterations increases. In terms of computational efficiency the DPDFT avoids the costly creation and inversion of a 2521×2521 complex P matrix needed to compute the PDFT, but the DPDFT cannot obtain a comparable resolution like the PDFT estimate unless it completes 15 iteration or more. The iterative process of the DPDFT is typically subject to the problem of the slow convergence observed in Figure 3(a), which may outweigh the cost in time and memory associated with the setup and inversion of the P-matrix.

For the same data used for the example in Figure 2, we computed the image by implementing the random permutation scheme (RPS) and the Herman-Meyer scheme (HMS) [14] to adjust the data access order for the DPDFT. It is remarkable that the DPDFT estimate after one iteration with RPS reordering, in Figure 4(a), and with HMS reordering, in Figure 4(b), show comparable resolution as compared to the DPDFT estimate after 15 iterations and without reordering, in Figure 2(f). The quantitative improvement of the DPDFT by using either the RPS, or the HMS reordering is illustrated in Figure 3(b) and Figure 3(c) respectively. As compared with Figure 3(a), Figure 3(b) and Figure 3(c), improves the convergence rate dramatically essentially approaching the final accuarcy after about three iterations. However, the

in both cases the RMSE remains slightly above the value for the PDFT estimate. Since our implementation of the PDFT algorithms incorporates a Miller-Tikhonov regularization [19] step, the solution does not represent the minimum weighted norm approximation in a rigorous sense and a small deviation between the reconstructions computed with DPDFT and PDFT is expected.

From the image in Figure 4(d), we see that by choosing a relaxation parameter of 0.09 the DPDFT estimate requires only 3 iterations to improve to a resolution comparable to the DPDFT estimate after 15 iterations, but with no reordering and no relaxation (Figure 2(f)). If we apply one of the schemes to change the data access order simultaneously to applying the relaxation parameter, we obtain a solution comparable to the ones in Figures 2(f) and 4(d) after only one iteration. In addition, we found that the use of reordering schemes extends the range for the relaxation parameter for which we obtain optimum performance (Figure 5). In practice, this yields significantly higher stability, since the results obtained with the DPDFT are less sensitive to choice of the regularization parameter.

4. Regularization of the DPDFT

If the measured data are noisy, the iterative process of the DPDFT will typically converge to a poor solution of very large energy. For explanation, we consider the same example in Figure 2, but using noisy Fourier data. The noise sources considered here are simulated by Gaussian white noise. Leaving all other parameters unchanged

the PDFT estimate must be regularized to recover a good estimate. For the PDFT algorithm with a Miller-Tikhonov regularization, the diagonal of the P-matrix is multiplied with a factor $\epsilon = 1 + \kappa$, with $\kappa \ll 1$ typically. Among all computed PDFT results we found the regularization value $\kappa = 0.5$ to yield the smallest RMSE. The corresponding image estimate is shown in Figure 6(a).

Likewise, in the case of noisy data the DPDFT cannot give a good estimate without regularization. The RMSEs between the object and the DPDFT estimates are shown in Figure 7(a). The resolution of the DPDFT estimates improves gradually as the number of iterations increases. For more than 8 iterations, however, the RMSE again increases. Both the DPDFT estimate after 8 iterations (Figure 6(b)), and the DPDFT estimate after 20 iterations (Figure 6(c)) show poor resolution, which highlight the impact of noise on the performance of the DPDFT. The poor convergence due to noise can be addressed with suitable regularization methods. We now summarize a method for regularizing the DPDFT algorithm.

The underdetermined system of linear equations $\mathbf{Bg} = \mathbf{d}$ always has multiple solutions, even with noiseless data. Usually, the minimum norm solution is used to select a unique solution. It was shown that the ART converges to the minimum norm solution of the system of equations, if it is implemented with a sequence of relaxation parameters $\lambda^k \in (0, 2)$ converging to zero and the initial vector $\mathbf{f}^0$ is in $\mathbb{S}(\mathbf{A}^T)$ [17,18].

Mathematically, $\mathbb{S}(\mathbf{A}^T)$ can be represented as

$$\mathbb{S}(\mathbf{A}^T) = \{\mathbf{v} | \mathbf{v} = \sum_{n=1}^{N} \alpha_n (\mathbf{A}^T)_{n-col}, \text{ for some arbitrary real numbers } \alpha_n\} , \qquad (17)$$

where $(\mathbf{A}^T)_{n-col}$ denotes the n-th column vector of the matrix $\mathbf{A}^T$. Typically, the origin is chosen as the initial vector, i.e. $\mathbf{f}^0 = \mathbf{0}$. However, in the presence of noisy data, even this minimum norm solution can have a large norm and does not correspond to a useful reconstruction. Regularizing this scheme typically involves rejecting exact solutions of $\mathbf{Af} = \mathbf{d}$ and seeking instead a vector $\hat{\mathbf{f}}$, which minimizes the function $\|\mathbf{Af} - \mathbf{d}\|^2 + \epsilon^2 \|\mathbf{f}\|^2$, with $\epsilon > 0$ being small [20]. The method due to the regularization uses the ART to solve the system of equations given in the matrix equation by

$$\begin{bmatrix} \mathbf{A} & \epsilon\mathbf{I} \end{bmatrix} \begin{bmatrix} \mathbf{f} \\ \\ \mathbf{v} \end{bmatrix} = \mathbf{d} . \qquad (18)$$

For the ART iterative process of equation (18), we begin at $\mathbf{f}^0 = \mathbf{0}$ and $\mathbf{v}^0 = \mathbf{0}$, then the limit for its upper component $\mathbf{f}^\infty = \hat{\mathbf{f}}$. The iterative step can be represented as

$$f_n^{k+1} = f_n^k + p_n \overline{A}_{mn} \left(\frac{d_m - \sum_{i=1}^{N} A_{mi} f_i^k - \epsilon v_m^k}{\epsilon^2 + \sum_{i=1}^{N} p_i |A_{mi}|^2} \right) \qquad (19)$$

$$v_m^{k+1} = v_m^k + \epsilon \left(\frac{d_m - \sum_{i=1}^{N} A_{mi} f_i^k - \epsilon v_m^k}{\epsilon^2 + \sum_{i=1}^{N} p_i |A_{mi}|^2} \right) , \qquad (20)$$

where

$$v_j^{k+1} = v_j^k \qquad \text{for} \qquad j \neq \text{mod}(k, M) + 1 \, . \tag{21}$$

Then the reconstructed image is the limit of the sequence $\{\mathbf{f}^k\}$.

To illustrate this, we again consider the same example as used in Figure 6, where the DPDFT did not converge significantly during the first 8 iterations, but diverged as the number of iterations increased. The result after 8 iterations still looks poor as compared to the PDFT estimate in Figure 6(a).

When we apply the regularization method (Figure 6(d)), the DPDFT clearly converges after 10 iterations and the resulting image is comparable to the PDFT estimate in Figure 6(e). The RMSEs as shown in Figure 7(b) confirms the superior convergence of the DPDFT using regularization.

Further improvement is again observed by combining the regularization method with a changed data access order. The resulting RMS values are plotted in Figure Figures 8(a) and 8(b). The convergence is significantly improved. Equally remarkable, the final RMS value is slightly better than that of the PDFT estimate. The corresponding image estimates are shown in Figures 6(e) and (f), which confirm an image quality comparable to the PDFT estimate in Figure 6(a) and the DPDFT estimate in Figure 6(d).

5. Conclusion

We described the discrete implementation of the PDFT algorithm. The PDFT algorithm and its discrete counterpart, the DPDFT algorithm, are typically used to compute image estimates from projection data. Both algorithms allow one to incorporate prior knowledge about the imaging problem to improve the reconstructed image.

The DPDFT algorithm was primarily implemented as a substitute for the well-explored PDFT algorithm, which does not require the inversion of the P-matrix. If the optimum reconstruction can be obtained with a few iterations of the DPDFT this invariably provides a speed-up as compared to the implementation of the PDFT algorithm, which increases with the size of the data set. However, the more important application of the DPFT is with respect to data sets which are too large to allows for the inversion of the corresponding P-matrix.

In addition, we emphasize that the DPDFT algorithm eliminates the need to compute the Fourier transformation of the prior in order to obtain a reconstruction of the object. This property is particularly useful, if the prior is not given in analytic form, but is the result of a pre-processing step and is only available in discrete form. In this case the DPDFT algorithm is the method of choice to obtain a constraint image estimate of the object. It is noted, however, that even if the prior is available in analytic form the computation of the P-matrix can contribute significantly to

the computational burden of the PDFT algorithm, and the DPFT provides a more efficient use of the prior information.

In our examples, the DPDFT was implemented using the ART algorthm, although this is not essential, and we make no assertions for or against the ART. We demonstrated that the convergence speed can be improved by reordering, which was successfully applied to ART related reconstruction schemes in the past. In particular, we investigated changing the access order of individual elements of the system of linear equations which needs to be solved. Independently of the access order scheme chosen, we found significant improvement of the convergence.

For noisy data it proved necessary to implement a suitable regularization method. Again, the behavior of the DPDFT algorithm proved sufficiently similar to previously described variants of the ART to adapt a known regularization scheme for use with the DPDFT algorithm. Our results show that this allows us to address noise related imaging problems effectively.

References

1. C. L. Byrne and R. M. Fitzgerald, "Reconstruction from partial information, with applications to tomography," SIAM J. Appl. Math. **42**, 933–940 (1982).
2. C. L. Byrne, R. M. Fitzgerald, M. A. Fiddy, T. J. Hall, and A. M. Darling, "Image restoration and resolution enhancement," J. Opt. Soc. Am. **73**, 1481–1487 (1983).
3. C. L. Byrne and R. M. Fitzgerald, "Spectral estimators that extend the maximum

entropy and maximum likelihood methods," SIAM J. Appl. Math. **44**, 425–442 (1984).

4. C. L. Byrne and M. A. Fiddy, "Image as power spectral; reconstruction as a Wiener filter approximation," Inverse Problems **4**, 399–409 (1988).

5. H. M. Shieh, C. L. Byrne, and M. A. Fiddy, "Image reconstruction: a unifying model for resolution enhancement and data extrapolation (TUTORIAL)," (2005). Accepted by J. Opt. Soc. Am. A.

6. C. L. Byrne, *Signal Processing: A Mathematical Approach* (AK Peters, Ltd., Wellesley, MA, 2005).

7. S. Kaczmarz, "Angenaherte auflosung von system linearer gleichungen," Bulletin de l'Academie Polonaise des Sciences et Lettres **A35**, 355–357 (1937).

8. R. Gordon, R. Bender, and G. T. Herman, "Algebraic reconstruction techniques (ART) for three-dimensional electron microscopy and x-ray photography," Journal of Theoretical Biology **29**, 471–481 (1970).

9. K. Tanabe, "Projection method for solving a singular system of linear equations and its applications," Numer. Math. **17**, 203–214 (1971).

10. R. Gordon, "A tutorial on ART," IEEE Transactions on Nuclear Science **NS-21**, 78–93 (1974).

11. G. T. Herman and A. Lent, "Iterative Reconstruction Algorithms," Comput. Biol. Medicine **6**, 273–294 (1976).

12. G. T. Herman and H. K. Tuy, "Image reconstruction from projections: an approach from mathematical analysis," in *Basic methods of tomography and inverse problems*, P. C. Sabatier, ed., pp. 1–124 (Adam Hilger, 1987).

13. G. T. Herman, *Image reconstruction from projections: the fundamentals of computerized tomography* (Academic Press, New York, 1980).

14. G. T. Herman and L. B. Meyer, "Algebraic reconstruction techniques can be made computationally efficient," IEEE transactions on medical imaging **MI-12**, 600–609 (1993).

15. H. Guan and R. Gordon, "A projection access order for speedy convergence of ART (algebraic reconstruction technique): a multilevel scheme for computed tomography," Phys. Med. Biol. **39**, 2005–2022 (1994).

16. G. T. Herman, "A relaxation method for reconstructing objects from noisy X-rays," Math. Prog. **8**, 1–19 (1975).

17. G. T. Herman, A. Lent, and P. H. Lutz, "Relaxation methods for image reconstruction," Commun. Assoc. Comput. Mach. **21**, 152–158 (1978).

18. M. R. Trummer, "Reconstructing pictures from projections: on the convergence of the ART algorithm with relaxation," Computing **26**, 189–195 (1981).

19. M. Bertero and P. Boccacci, *Introduction to Inverse Problems in Imaging* (IOP Publishing, Bristol, 1998).

20. P. Eggermont, G. T. Herman, and A. Lent, "Iterative Algorithms for Large Par-

titioned Linear Systems, with Applications to Image Reconstruction," Linear Algebra and its Applications **40**, 37–67 (1981).

List of Figure Captions

Fig. 1. Illustration of the Fourier spaces mapping of the simulated data.

Fig. 2. The reconstruction of an object of compact support: (a) the object, (b) the discrete Fourier transform estimate, (c) circular flat-top used as prior function, (d) the PDFT estimate, (e) the DPDFT estimate after 6 iterations, and (f) the DPDFT estimate after 15 iterations.

Fig. 3. The RMSEs between the original and the reconstructed image for simulated noiseless Fourier data: (a) the RMSEs for the PDFT and the DPDFT after 1-20 iterations, (b) same as in (a) applying the RPS reordering, and (c) same as in (a) applying HMS reordering.

Fig. 4. The reconstruction of an object with compact support using the DPDFT with reordering and relaxation (a) 1-iteration DPDFT estimate with RPS reordering, and (b) 1-iteration DPDFT estimate with HMS reordering, (c) 1-iteration DPDFT estimate with the relaxation parameter 0.07, and (d) 3-iteration DPDFT estimate with the relaxation parameter 0.09.

Fig. 5. Impact of the relaxation parameter on the RMSEs: (a) the RMSEs for the PDFT and the DPDFT after three iterations with no reordering, (b) same for the DPDFT after one iteration with RPS reordering, and (c) same for the DPDFT after one iteration with HMS reordering.

Fig. 6. The reconstruction of an object of compact support from the noisy data: (a) the

PDFT estimate with regularization value of $\kappa = 0.5$, (b) the DPDFT estimate after 8 iterations, (c) the DPDFT estimate after 20 iterations, (d) the DPDFT estimate after 10 iterations with regularization value of $\epsilon = 0.7$, (e) the DPDFT estimate after one iteration with regularization value of $\epsilon = 0.7$ and RPS reordering, and (f) the DPDFT estimate after one iteration with regularization value of $\epsilon = 0.7$ and HMS reordering.

Fig. 7. The RMSEs between object and image computed from simulated noisy data: (a) the DPDFT estimate without regularization, (b) the DPDFT estimate with regularization value of $\epsilon = 0.7$.

Fig. 8. The RMSEs between object and image for simulated noisy data: (a) RPS reordering and regularization value of $\epsilon = 0.7$, and (b) HMS reordering and regularization value of $\epsilon = 0.7$.

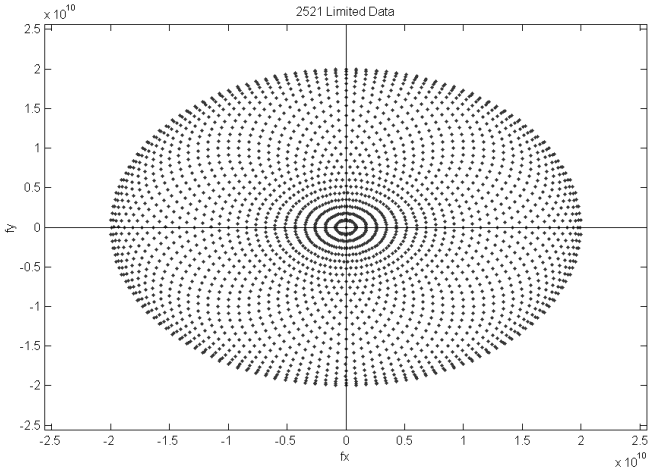

Fig. 1. Illustration of the Fourier spaces mapping of the simulated data. Shieh_fmap.eps

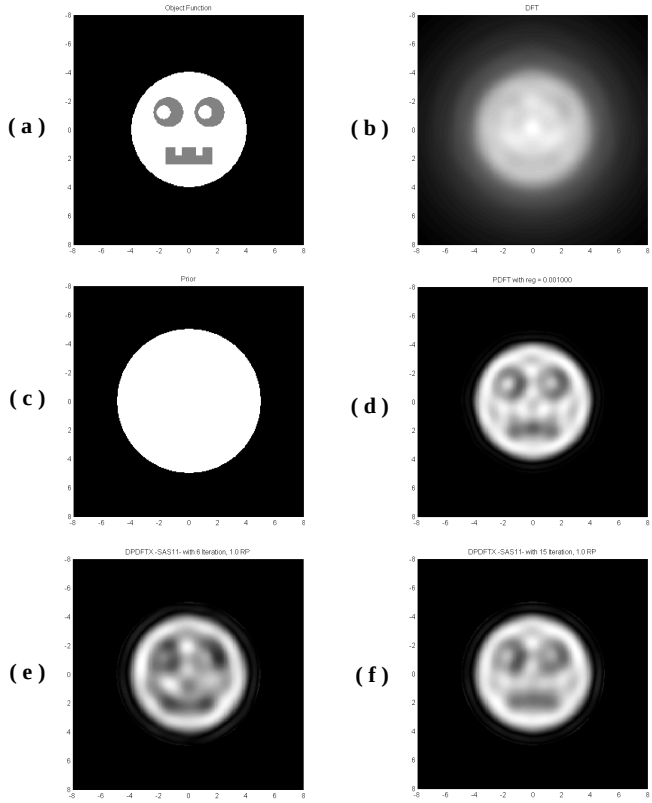

Fig. 2. The reconstruction of an object of compact support: (a) the object, (b) the discrete Fourier transform estimate, (c) circular flat-top used as prior function, (d) the PDFT estimate, (e) the DPDFT estimate after 6 iterations, and (f) the DPDFT estimate after 15 iterations. Shieh_estimate01.eps

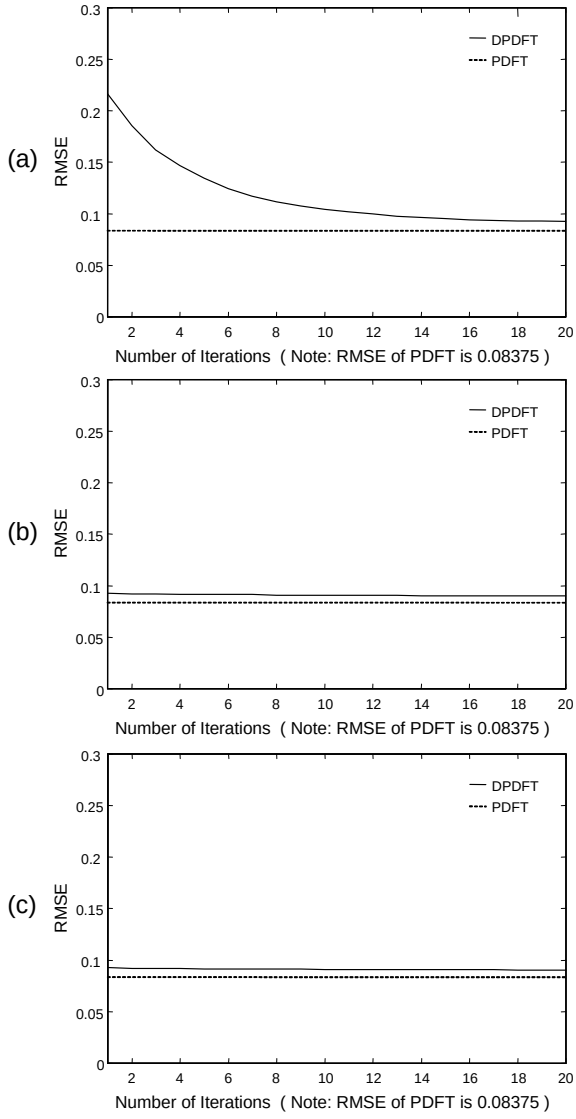

Fig. 3. The RMSEs between the original and the reconstructed image for simulated noiseless Fourier data: (a) the RMSEs for the PDFT and the DPDFT after 1-20 iterations, (b) same as in (a) applying the RPS reordering, and (c) same as in (a) applying HMS reordering. Shieh_ed01.eps

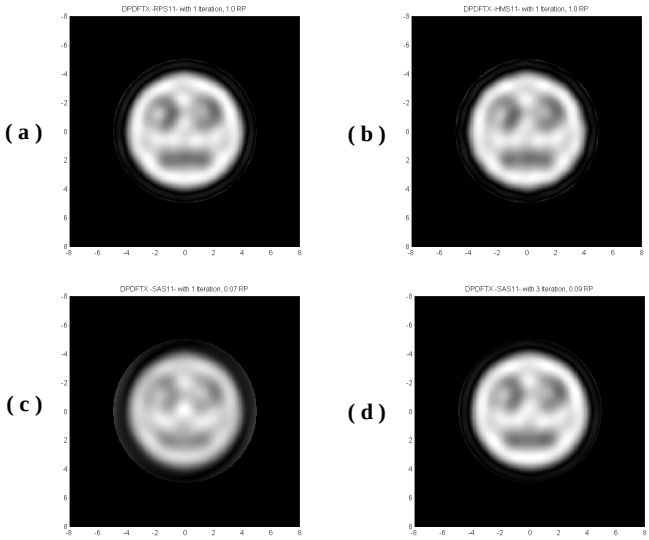

Fig. 4. The reconstruction of an object with compact support using the DPDFT with reordering and relaxation (a) 1-iteration DPDFT estimate with RPS reordering, and (b) 1-iteration DPDFT estimate with HMS reordering, (c) 1-iteration DPDFT estimate with the relaxation parameter 0.07, and (d) 3-iteration DPDFT estimate with the relaxation parameter 0.09. Shieh_estimate02.eps

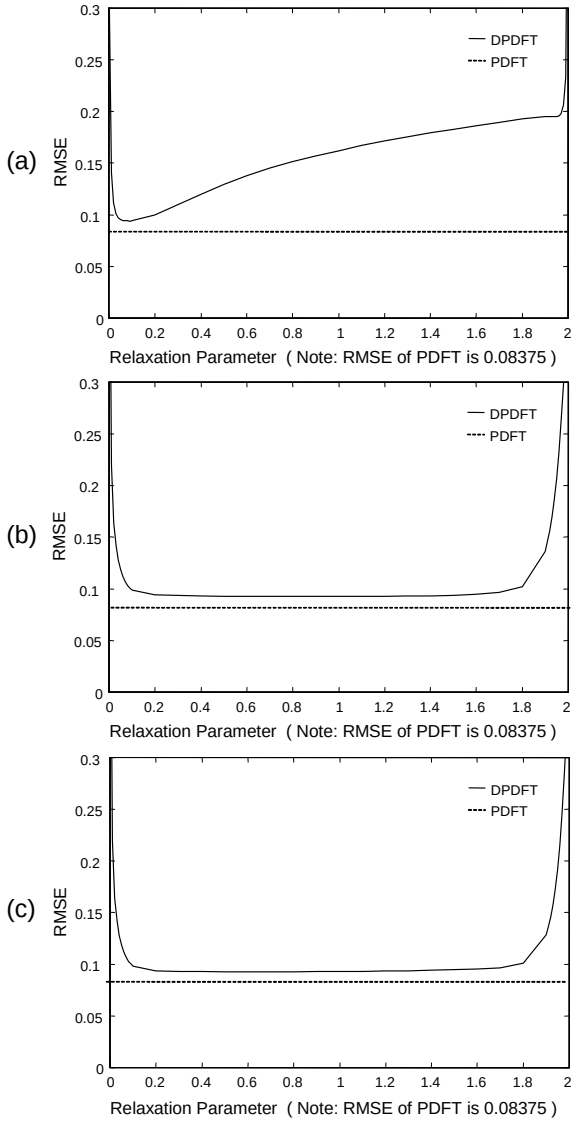

Fig. 5. Impact of the relaxation parameter on the RMSEs: (a) the RMSEs for the PDFT and the DPDFT after three iterations with no reordering, (b) same for the DPDFT after one iteration with RPS reordering, and (c) same for the DPDFT after one iteration with HMS reordering. Shieh_ed02.eps

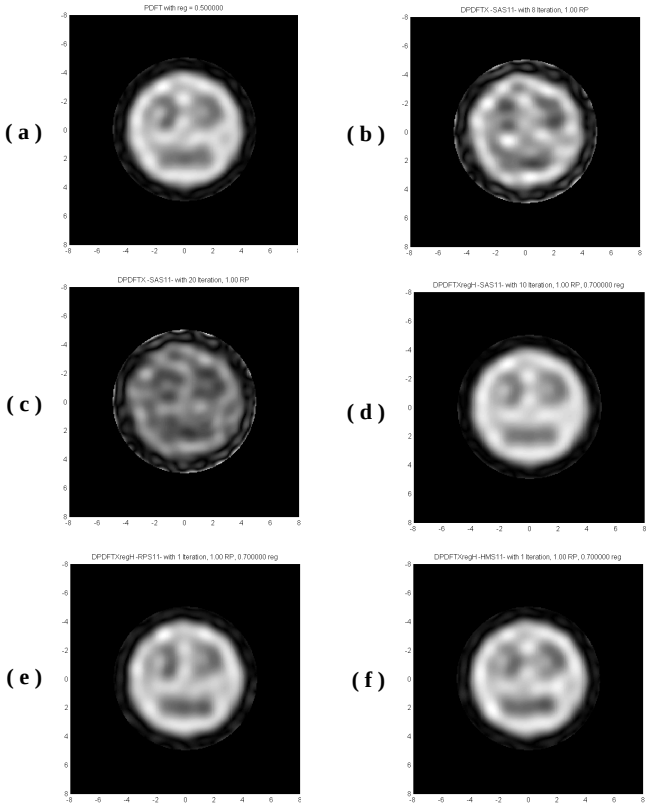

Fig. 6. The reconstruction of an object of compact support from the noisy data: (a) the PDFT estimate with regularization value of $\kappa = 0.5$, (b) the DPDFT estimate after 8 iterations, (c) the DPDFT estimate after 20 iterations, (d) the DPDFT estimate after 10 iterations with regularization value of $\epsilon = 0.7$, (e) the DPDFT estimate after one iteration with regularization value of $\epsilon = 0.7$ and RPS reordering, and (f) the DPDFT estimate after one iteration with regularization value of $\epsilon = 0.7$ and HMS reordering. Shieh_estimate03.eps

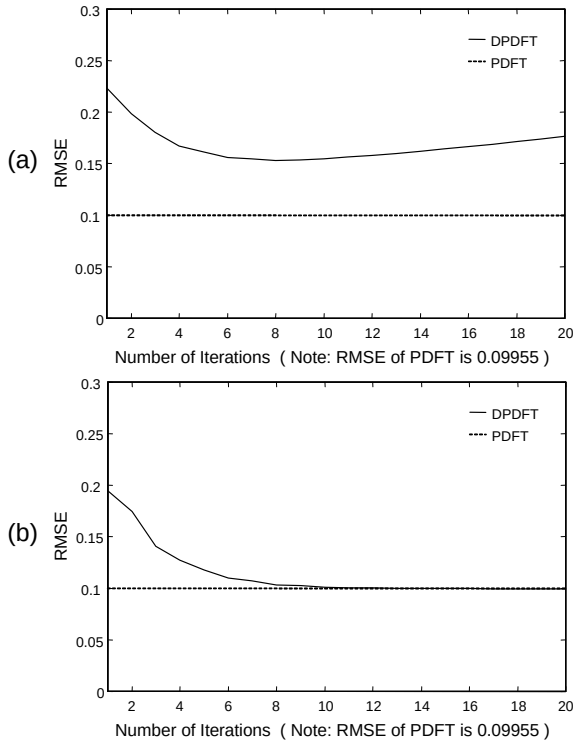

Fig. 7. The RMSEs between object and image computed from simulated noisy data: (a) the DPDFT estimate without regularization, (b) the DPDFT estimate with regularization value of $\epsilon = 0.7$. Shieh_ed03.eps

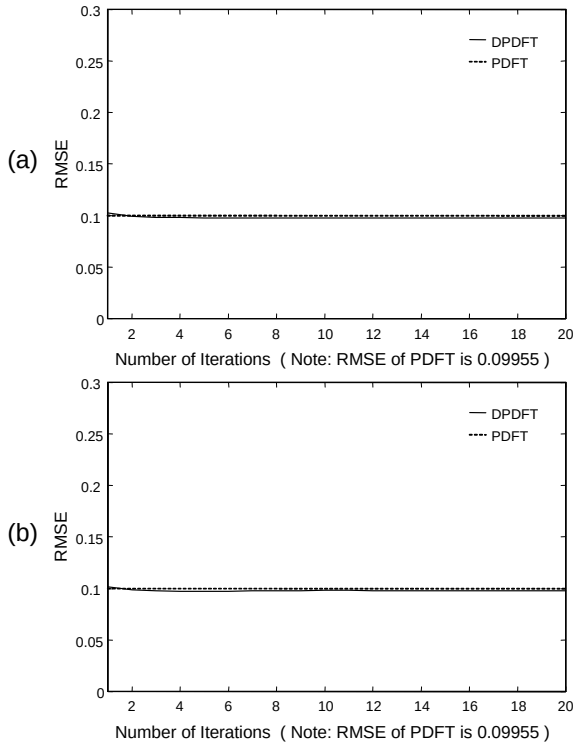

Fig. 8. The RMSEs between object and image for simulated noisy data: (a) RPS reordering and regularization value of $\epsilon = 0.7$, and (b) HMS reordering and regularization value of $\epsilon = 0.7$. Shieh_ed04.eps